ELSEVIER

Fuel 78 (1999) 259–270

FUEL

Hydrobiogeochemical interactions in 'anoxic' limestone drains for neutralization of acidic mine drainage

E.I. Robbins[a,*], C.A. Cravotta III[b], C.E. Savela[c], G.L. Nord Jr.[a]

[a]*US Geological Survey, National Center MS 956, Reston, VA 20192, USA*
[b]*US Geological Survey, 840 Market Street, Lemoyne, PA 17043, USA*
[c]*USDA-Natural Resources Conservation Service, 75 High Street, Room 301, Morgantown, WV 26505, USA*

Received 9 December 1997; received in revised form 29 May 1998

Abstract

Processes affecting neutralization of acidic coal mine drainage were evaluated within 'anoxic' limestone drains (ALDs). Influents had pH $\leq$ 3.5 and dissolved oxygen $<$ 2 mg/l. Even though effluents were near neutral (pH $>$ 6 and alkalinity $>$ acidity), two of the four ALDs were failing due to clogging. Mineral-saturation indices indicated the potential for dissolution of calcite and gypsum, and precipitation of Al^{3+} and Fe^{3+} compounds. Cleavage mounts of calcite and gypsum that were suspended within the ALDs and later examined microscopically showed dissolution features despite coatings by numerous bacteria, biofilms, and Fe–Al–Si precipitates. In the drain exhibiting the greatest flow reduction, Al-hydroxysulfates had accumulated on limestone surfaces and calcite etch points, thus causing the decline in transmissivity and dissolution. Therefore, where Al loadings are high and flow rates are low, a pre-treatment step is indicated to promote Al removal before diverting acidic mine water into alkalinity-producing materials. Published by Elsevier Science Ltd.

Keywords: Aluminite; Biofilms; Epilithic bacteria; Gibbsite; Limestone armoring; Anoxic limestone drains; Acid mine drainage

1. Introduction

Many techniques are being developed to treat acidic mine drainage (AMD). In the subsurface, various natural and man-made alkaline materials have been tested for their neutralization potential; these include coal combustion byproducts (CCBs)[1, 2], flue gas desulfurization byproducts (FGDBs) [3], and oxic and anoxic limestone drains (ALDs) [4–6].

CCBs and FGDBs are heterogenous materials composed of oxide, carbonate, silicate, and sulfate minerals [2, 3]. Built at the outflows of acidic drainage, ALDs are trenches filled solely with limestone gravel that dissolves to add alkalinity [4, 5]. ALDs are covered to retain CO_2 and exclude O_2 in order to maximize limestone dissolution, minimize oxidation and hydrolysis of iron, and avoid formation of iron-hydroxide coatings on the limestone [7]. Some ALDs fail within months as the gravel becomes clogged, plugged, or armored with iron and aluminum hydroxide minerals and slimes [8]. The nature and effects of minerals that form in ALDs are not well known. Poorly crystalline compounds of Fe, Al, S, and Si have been identified in pH-adjusted artificial mixtures with AMD [9–13], in soils affected by mining [14, 15], and in association with bacteria from AMD waters [16].

Chemical equations can be written for a variety of potential products that might form from mixing AMD and alkalinity-producing substances in the subsurface environment. Rates of calcite dissolution and precipitation are directly pH dependent [17–19]. However, little is known about effects of heterogenous CCBs and FGDBs on $CaCO_3$ dissolution. Theoretical scenarios can be defended to show that alkalinity production could be either decreased or increased by addition of these byproducts to limestone-utilizing AMD treatment systems. Owing to elevated SO_4^{2-}, SiO_2, and Al^{3+} from byproducts, secondary minerals such as gypsum or gibbsite could form by reactions with products of $CaCO_3$ dissolution and retard dissolution. This means that alkalinity production could be decreased if such secondary minerals coat $CaCO_3$ surfaces. Alternatively, the removal of Ca^{2+} from solution by gypsum precipitation could decrease the ion activity product of calcite and promote $CaCO_3$ dissolution, thus increasing alkalinity. Likewise, silicates in CCBs or FGDBs may be active in ion exchange, removing Ca^{2+} from solution and hence promoting $CaCO_3$ dissolution.

While water sampling and geochemical calculations can

* Corresponding author. Tel.: + 1-703-6486527; Fax: + 1-703-6486419; e-mail: nrobbins@usgs.gov.

0016-2361/98/$ - see front matter Published by Elsevier Science Ltd.
PII: S0016-2361(98)00147-1

indicate the chemical environment, microscopic methods can indicate the microbial consortium that is active under the actual conditions. Culturing and genetic techniques are standard methods for subsurface microbial studies [20]. However, culturing tends to grow bacteria amenable to the growth medium and genetic analysis requires batch culturing to learn the specific identity of the bacteria actually analyzed. In contrast, direct observation of subsurface bacterial populations allowed us to assess the intimate interactions between the bacteria and the minerals formed.

A major objective of our work was to evaluate the dissolution of calcite and gypsum and precipitation of secondary mineral products in order to understand reactions in the subsurface. We conducted field experiments in ALDs in West Virginia and Pennsylvania. We report on direct microscopic methods (microbiology and mineralogy) and indirect aqueous chemical methods to evaluate potential for dissolution and precipitation. We then discuss the implications of this research on individual components to the use of heterogenous alkalinity-producing materials such as CCBs and FGDBs for AMD treatment.

2. Study sites

In West Virginia, three ALDs were built in 1992 by the USDA-Natural Resources Conservation Service as part of Rural Abandoned Mine Program (RAMP) to capture AMD from old adits and seeps from an underground mine complex in the Pittsburgh coal bed. This Ridenour RAMP site is 8.5 km northeast of Morgantown (lat. 39°42′57″N, long. 79°54′12″W). Each ALD was constructed by burying more than 100 000 kg of limestone gravel (90% $CaCO_3$, ≤2.5 cm) in 21–25-m long trenches that were wrapped with plastic and then buried under 0.5–2 m of soil [8, 21]. Stand pipes at the outlets maintain water levels so the limestone is continuously submerged. During construction, capped PVC monitoring ports were installed within each drain. Wire cages filled with limestone gravel were suspended in the ports to evaluate water–mineral reactions. Because of subsequent coating of the limestone by variously colored secondary precipitates, the ALDs are designated the 'Red drain', the 'Black drain', and the 'White drain'. In the Red drain, the limestone became coated with a hydrous iron oxide and, concurrently, transmissivity decreased. In the Black drain, the limestone became coated with a black iron sulfide that did not impede flow. The White drain began to clog within 6 months due to the formation of a gummy white precipitate on the gravel and within pore spaces. The white precipitate was identified as a poorly crystalline Al-hydroxysulfate mineral that displays broad irregular maxima in a X-ray diffraction pattern having *d*-spacings similar to the three most intense lines of aluminite [$Al_2(SO_4)(OH)_4 \cdot 7H_2O$] [8, 22].

In Pennsylvania, three identical, parallel limestone drains were constructed in 1995 to treat AMD from the Orchard Mine in the Llewellyn Formation of the Southern Anthracite coalfield. This Orchard Overflow site is 6 km south of Tremont (lat. 40°36′26″N, long. 76°25′30″W). Approximately 12 700 kg of tabular limestone fragments (97% $CaCO_3$, 3 × 10 cm) were placed in each 30 m long trench and wrapped completely with plastic before backfilling to the original land-surface grade [23, 24]. Sealed PVC monitoring pipes were installed at the drain inflows, at points within the drains, and at their outflows. Although limestone surfaces near the inflow to the drains became coated with iron hydroxide and minor amounts of Al- and Mn-bearing compounds, the drains are fully functional.

3. Experimental

3.1. Water sampling and analytical methods

Temperature, specific conductance (SC), dissolved O_2 (DO), pH, and redox potential (Eh) were measured electrometrically, downhole or in flow cells, using standard field methods [25, 26]. Water samples were collected with a peristaltic pump while maintaining a constant flow rate through each ALD. Alkalinity and cold acidity of unfiltered samples were titrated in the field [13, 21, 27]. Filtered (0.45 μm; acidified) and unfiltered (acidified and non-acidified) subsamples were processed in the field for laboratory analysis of Al, Ca, Fe, K, Mg, Mn, Na, SiO_2, and SO_4 by standard methods [27].

Partial pressures of CO_2 (P_{CO_2}), activities of aqueous species, and mineral saturation indices were calculated using the results of water analyses and the WATEQ4F computer program [28]. The saturation index ($SI = \log(IAP/K_T)$, where K_T is the solubility product constant and IAP is the corresponding observed activity product) provides a basis for evaluating the potential for dissolution or precipitation of a solid phase by the sampled water [28]. Thermodynamic data were not available in WATEQ4F for aluminite or schwertmannite [$Fe_8O_8(OH)_6SO_4$], so SI values for these minerals could not be computed. Data for basaluminite, ferrihydrite, and other possible secondary minerals are reported (Table 1). Values of SI that are negative (≤−0.1), zero (±0.1), or positive (>0.1) indicate the water is undersaturated, saturated, or supersaturated, respectively, with the solid phase. If undersaturated, the water can dissolve the solid phase. If supersaturated, the water cannot dissolve the solid phase, but can potentially precipitate it.

3.2. Microscopic methods

Epilithic bacteria (those attached to solid surfaces), flocculate bacteria (those associated with loose flocculate), and mineral precipitates were collected on submerged glass microscope slides (controls) and cleavage mounts of transparent calcite and gypsum affixed to glass microscope slides. This new technique for sampling subsurface epilithic bacteria was modified from Zobell [29] and Mills and

Table 1
Water composition and calculated saturation indices at inflow and downflow through limestone drains in Pennsylvania and West Virginia Constituents are dissolved and units are mg/l, except as noted; $<$, less than; n.d., no data.

Parameter or constituent	West Virginia, 16 April 1997									Pennsylvania, 16 August 1995						
	Black Drain			Red Drain			White Drain			Inflow	Drain 1			Drain 2		
Distance (m) (*, outflow location)	0	3.0	21.3*	0	3.0	21.3*	0	15.2	25.0*	0	6.1	12.2	24.4*	6.1	12.2	24.4*
Residence time (h)[a]	0	49	344	0	22	151	0	9	23	0	0.4	0.8	1.6	0.4	0.8	1.6
Specific conductance (μS/cm)	1,360	1,450	1,540	2,940	1,870	2,820	1,500	2,000	1,670	430	390	420	620	380	420	630
Eh (mV)	490	120	150	700	590	230	680	620	220	710	430	410	400	420	410	400
pH (units)	3.5	6.3	6.1	2.4	3.5	6.3	3.0	3.3	6.0	3.4	5.3	6.0	6.8	5.3	6.1	6.8
Acidity, as $CaCO_3$	326	0	0	1390	508	0	268	310	0	56	23	21	<20	19	21	<20
Alkalinity, as $CaCO_3$	0	286	278	0	0	406	0	0	198	0	26	54	110	19	56	113
SO_4	710	550	660	1,940	1,550	1,530	900	990	850	240	220	220	220	220	220	220
Ca	54	212	219	64	143	571	154	154	302	29	49	57	79	50	63	78
SiO_2	52.4	41.1	41.5	88.0	46.9	8.5	43.4	47.7	34.0	9.7	9.8	9.6	9.7	10.0	9.9	9.4
Al	16.7	<0.14	<0.14	104	48.2	<0.14	34.3	46.1	0.19	0.83	0.29	0.12	0.03	0.30	0.05	0.02
Fe	79	61.5	87.5	188	22.3	55.4	1.86	2.47	5.64	1.37	0.03	0.01	<0.01	0.08	0.02	0.01
Mn	6.6	6.5	7.5	9.1	47.0	11.0	32.4	32.7	32.5	3.0	3.1	3.0	2.9	3.2	3.1	2.9
Saturation index (unitless)[b]																
Calcite ($CaCO_3$)	n.d.	−0.7	−1.0	n.d.	n.d.	−0.4	n.d.	n.d.	−1.0	n.d.	−3.2	−2.1	−0.9	−3.4	−2.0	−0.9
Gypsum ($CaSO_4{\cdot}2H_2O$)	−1.2	−0.7	−0.6	−1.0	−0.7	−0.1	−0.7	−0.7	−0.4	−1.6	−1.4	−1.4	−1.3	−1.4	−1.3	−1.3
Siderite ($FeCO_3$ ppt)	n.d.	0.6	0.5	n.d.	n.d.	0.5	n.d.	n.d.	−0.9	n.d.	−4.5	−4.0	−4.5	−4.3	−3.9	−4.1
Ferrihydrite [$Fe(OH)_3$]	−2.2	−0.6	−0.6	−2.1	−1.1	1.0	−2.5	−2.2	−0.7	−0.9	−1.2	−0.1	0.6	−1.2	0.3	0.9
Goethite (FeOOH)	1.3	2.9	2.9	1.4	2.4	4.5	1.0	1.4	2.8	2.6	2.3	3.4	4.1	2.3	3.8	4.4
Jarosite [$(H_3O,K,Na)Fe_3(SO_4)_3(OH)_6$]	−3.5	−7.9	−7.0	0.2	0.4	−2.6	−2.4	−2.5	−7.0	−0.4	−7.4	−6.3	−6.9	−7.1	−5.4	−5.9
SiO_2, amorphous	−0.2	−0.3	−0.3	−0.0	−0.3	−1.0	−0.3	−0.3	−0.4	−1.0	−1.0	−1.0	−1.0	−1.0	−1.0	−1.0
$Al(OH)_3$, amorphous	−5.5	−1.8	−2.6	−8.3	−5.3	−1.1	−7.1	−6.1	−2.3	−6.9	−1.8	−0.8	−0.6	−2.0	−1.1	−0.7
Gibbsite [$Al(OH)_3$]	−2.7	1.1	0.3	−5.5	−2.5	1.7	−4.2	−3.2	0.6	−4.1	1.0	2.0	2.2	0.8	1.7	2.1
Allophane $[Al(OH)_3]_{(1-x)}(SiO_2)_x]$	−0.8	0.7	0.2	−0.5	−0.8	0.9	−1.0	−0.9	0.3	−1.7	0.0	0.8	1.3	−0.1	0.7	1.2
Kaolinite [$Al_2Si_2O_5(OH)_4$]	−2.4	5.0	3.4	−7.5	−2.0	5.0	−5.5	−3.4	3.8	−6.6	3.5	5.5	6.0	3.2	4.9	5.7
Jurbanite [$Al(SO_4)(OH){\cdot}5H_2O$]	−0.2	−2.0	−2.3	−0.5	0.3	−0.9	−0.3	0.1	−1.8	−1.6	−0.5	−0.8	−2.1	−0.5	−1.4	−2.3
Basaluminite $[Al_4(SO_4)(OH)_{10}{\cdot}5H_2O]$	−7.5	2.1	−0.4	−16.1	−6.2	5.5	−11.8	−8.3	0.9	−13.2	3.0	5.6	5.2	2.6	4.2	4.6
Alunite [$KAl_3(SO_4)_3(OH)_6$]	−1.3	1.3	−0.2	−6.8	−0.1	3.8	−4.1	−2.0	0.9	−6.5	2.9	3.9	2.2	2.7	2.5	1.7
Log(P_{CO_2}) (atm)[b]	n.d.	−0.9	−0.7	n.d.	n.d.	−0.7	n.d.	n.d.	−0.8	n.d.	−0.9	−1.2	−1.7	−1.0	−1.3	−1.7

[a] For West Virginia drains, residence time computed as mass of limestone by bulk density (2200 kg/m^3) times porosity (0.14) and divided by flow rates of 0.03, 0.05 and 0.30 m^3/h, for Black, Red, and White drains, respectively, using mass and flow data from Hedin and Watzlaf [5]. For Pennsylvania drains, residence time computed as distance × cross-sectional area (0.23 m^2) × porosity (0.14) divided by volumetric flow rate of 0.5 m^3/h as reported by Cravotta and Trahan [24].

[b] Saturation index [SI = log(IAP/K_T)] and log(P_{CO_2}) calculated with WATEQ4F [28] using tabulated data for Eh, pH, and solute concentrations plus data for Mg, Na, K, Cl, and F; Al assumed to be at detection limit, if not detected. Temperature of samples ranged from 11.5 to 13.3°C. SI values for goethite computed using solubility reported by Bigham *et al.* [10], where log $K_{goethite} = 1.4$ (instead of −1.0 in WATEQ4F data base).

Table 2
Microbial and mineral components in ALDs Color abbreviations: bn, brown; bk, black; cr, creme; co, colorless; wh, white; yw, yellow. Other abbreviations: *L. disco*., *Leptothrix discophora*; —, not present; xx, not applicable

Site, sample number, and sample type		Sampling dates	pH (units)	Macroscopic characters	Dominant bacteria	Other	Dissolution features	New-formed minerals
West Virginia ALDs								
1	Red drain calcite slide (3.0 m)	3–23 Oct. 95	4.5	Opaque with yw film (10YR 7/8)	Bn short rods Fig. 3(9))		Pits and points (Fig. 2(3))	Ferrihydrite?, gypsum
2	Red drain glass slide (3.0 m)	3–23 Oct. 95	4.5	Slight yw film (10YR 7/8)	Co bifurcating rod filaments (Fig. 3(27)), cocci and long rods		xx	Ferrihydrite?, gypsum, co octahedrons
3	White drain calcite slide (15.2 m)	3–23 Oct. 95	4.0	Translucent with wh powder in patches	Co medium rods (Fig. 3(6))	Co biofilm	Pits and points with Al (Fig. 2(4)Fig. 2(5))	Aluminite, botryoidal red
4	White drain glass slide (15.2 m)	3–23 Oct. 95	4.0	Wh film	Co short rods	Wh biofilm	xx	–
5	Black drain calcite slide (3.0 m)	3–23 Oct. 95	7.0	Transparent	Bn short rods	Co biofilm; rosettes (Fig. 3(7))	–	Gypsum
6	Black drain glass slide (3.0 m)	3–23 Oct. 95 and Oct. 95–Oct. 96	7.0	Clear	Co and bn short rods	Wh biofilm	xx	Co blades, gypsum, prisms (Fig. 3(29)), pyrite
8	Red drain glass slide (3.0 m)	5 Mar.–22 Apr. 96	≈ 4.5	Yw film (10YR 7/8)	Bn short rods, co bifurcating rod filaments (Fig. 3(28)) and cocci		xx	Ferrihydrite? gypsum, co radiating, calcite
10	White drain glass slide (15.2 m)	5 Mar.–22 Apr. 96	≈ 4.0	Thick yw film (10YR 7/8)	Bn short rods (Fig. 3(22))	Cr biofilm	xx	Ferrihydrite?, co hexagons
11	Black drain gypsum slide (3.0 m)	5 Mar.–22 Apr. 96	≈ 7.0	Transparent	Co cocci and bn short rods	Co biofilm; *L. disco*. holdfasts (Fig. 3(14)); FeO_x spheres (Fig. 3(11))	Holes (Fig. 2(2))	Pyrite octahedrons
12	Black drain glass slide (3.0 m)	5 Mar.–22 Apr. 96	≈ 7.0	Clear	Co short rods	Bn and co biofilms; holdfasts (Fig. 3(25))	xx	Gypsum, co hexagons
27	Red drain slime (3.0 m)	18 Oct. 94	4.5	Brownish yw (10YR 6/8)	Bn and yw short rods (Fig. 3(15))		xx	Ferrihydrite?, gypsum
28	White drain slime (15.2 m)	18 Oct. 94 and 5 Oct. 96	4.0	Yw (10YR 7/8)	Yw cocci (Fig. 3(17))		xx	Aluminite, ferrihydrite? botryoidal red, pyrite
29	Black drain slime (3.0 m)	18 Oct. 94	7.0	Bk	Bk and bn medium rods (Fig. 3(16))		xx	Bk FeS, gypsum
Pennsylvania ALDs								
13	Inlet calcite slide (0 m)	19 Jul.–23 Aug. 95	3.4	Transparent with slight brownish yw film (10YR 6/8)	Bn short rods	Cr biofilm	–	Schwertmannite, goethite, gypsum
14	Inlet glass slide (0 m)	19 Jul.–23 Aug. 95	3.4	Brownish yw film (10 YR 6/8)	Bn short rods	Brownish yw biofilm; hyphae (Fig. 3(23)); *Gallionella*	–	Ferrihydrite?, schwertmannite, goethite, hollow prisms

15	Drain 1 calcite slide (6.1 m)	19 Jul.–23 Aug. 95	5.3	Transparent with brownish yw film (10YR 6/8)	Bn short rods	Cr and yw biofilms; *Gallionella*	Shatter cracks, pits and points	Ferrihydrite?, schwertmannite, goethite, gypsum
16	Drain 1 glass slide (6.1 m)	19 Jul.–23 Aug. 95	5.3	Thick brownish yw film (10YR 6/8)	Co and bn short rods (Fig. 3(24))	Brownish yw biofilm; *Gallionella*	xx	Ferrihydrite?, schwertmannite, goethite, gypsum (Fig. 3(26))
17	Drain 2 calcite slide (6.1 m)	19 Jul.–23 Aug. 95	5.3	Transparent with brownish yw, wh, and bk areas	Bn short rods (Fig. 3(10))	Cr and yw biofilms; bn fungi (Fig. 3(8))	Pits and points	Schwertmannite, goethite
18	Drain 2 glass slide (6.1 m)	19 Jul.–23 Aug. 95	5.3	White and brownish yw film (10YR 6/8)	Bn and co short rods (Fig. 3(21)); co long and medium rods	Yw biofilm	—	Schwertmannite, goethite, pyrite (Fig. 3(20))
19	Drain 1 calcite slide (6.1 m)	25 Oct. 95–26 Mar. 96	6.2	Opaque and coated brownish yw (10YR 6/8)	Bn short rods	Yw biofilm	Pyramids	Schwertmannite, goethite
20	Drain 1 glass slide (6.1 m)	25 Oct. 95–26 Mar. 96	6.2	Thick brownish yw in places (10YR 6/8)	Co and bn short rods	Cr and yw biofilm	xx	Schwertmannite, goethite
22	Drain 1 glass slide (6.1 m)	25 Oct. 95–26 Mar. 96	5.7	Brownish yw (10YR 6/8) and wh film	Co and bn short rods	Yw biofilm	–	Schwertmannite, goethite, gypsum
23	Drain 1 gypsum slide (12.2 m)	25 Oct. 95–26 Mar. 96	6.2	Transparent with brownish yw powder (10YR 6/8)	Bn short rods (Fig. 3(13)); cocci (Fig. 3(12))	Yw biofilm; fungal hyphae (Fig. 3(23))	Striations (Fig. 2(1))	Ferrihydrite?, schwertmannite?, Mn oxide
24	Drain 1 glass slide (12.2 m)	25 Oct. 95–26 Mar. 96	6.2	Brownish yw film (10YR 6/8)	Bn short rods	Yw biofilm; *Gallionella*	xx	Ferrihydrite?, schwertmannite, goethite, radiating blades
25	Yw-orange slime on limestone in Drains 1 and 2 (6.1 m)	20 Oct. 95	5.4	Yw orange slime	Bn short rods	*Gallionella* (Fig. 3(18))	xx	Ferrihydrite?, schwertmannite, goethite, gypsum, pyrite, calcite
26	Flocculate in pipe from mine (0 m)	20 Oct. 95	3.5	Yellowish bn (10YR 5/8)	Bn short rods (Fig. 3(19))		Cracks in gypsum crystals	Ferrihydrite? schwertmannite, goethite, gypsum (Fig. 3(26))

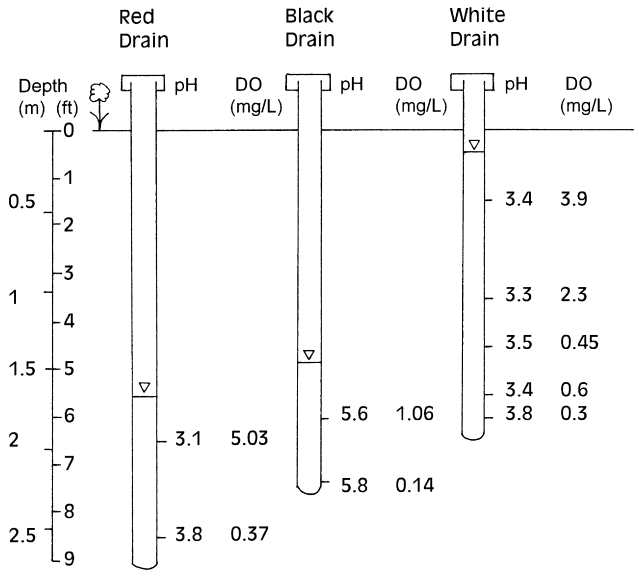

Fig. 1. Dissolved oxygen (DO), pH values, and water table elevation measured at different depths within the three West Virginia ALDs. (Red drain portal at 3 m from inflow, Black drain portal at 3.0 m, and White drain portal at 15.2 m; Date of collection, 16 Oct. 1996)

Mallory [30]. At the West Virginia sites, slide sets were suspended only in the mid-drain sampling ports, while at the Pennsylvania site, slides were suspended at the inflow and at points downflow in the ALDs. Time of immersion just above the bottom of the ports varied from less than 1 month to 1 year (Table 2). After retrieval, slides were air dried at room temperature, then dissolution features and precipitates and bacteria were analyzed using light and epifluorescent microscopy, scanning electron microscopy (SEM), X-ray energy-dispersive spectroscopy, and X-ray diffraction analysis. Iron bacteria were identified microscopically on the basis of morphological characteristics [31, 32].

4. Results and discussion

Water chemistry (Table 1, Fig. 1), precipitates on limestone, calcite, gypsum, and glass surfaces (Figs. 2 and 3), and microbial populations (Table 2, Fig. 3) were distinctive at each location and in each drain. The hydrochemical and microbial variations provide insight into the dynamic processes affecting acid neutralization and alkalinity production in constructed and natural systems.

4.1. Inflow rates and metal loading rates

The rates of flow varied among the ALDs. Flow through the West Virginia ALDs ranged from 0.5 l/min in the Black, 0.8 l/min in the Red, and 5 l/min in the White drains [5]. Flow through the Pennsylvania ALDs was 8.3 l/min. Hence, the residence or retention times for water differed greatly, from 1.6 h in the Pennsylvania to 23–344 h in the West Virginia ALDs (Table 1).

In general, Al and Fe precipitates formed in all the ALDs; however, declines in transmissivity were significant only for the ALDs receiving high metal loads. The metal load, which is the product of metal concentration and flow rate, differed among the ALDs. Aluminum loads were highest in the White (170 mg/min) ($=$ 34.3 mg/l $\times$ 5 l/min) and Red drains (83 mg/min), and lowest in the Black (8.35 mg/min) and Pennsylvania drains (6.8 mg/min). Clogging of the White and Red drains by Al and Fe compounds, respectively, is consistent with high loads and low flow rates, hence excessive accumulation of these metals occurred over a relatively short time.

4.2. Hydrochemical trends

Table 1 shows the untreated AMD diverted to each ALD was net acidic and had pH $\leq$ 3.5. The influents to the West Virginia ALDs were suboxic (DO $<$ 0.5 mg/l) and highly mineralized, with specific conductance (SC) ranging from 1360 to 2940 μS/cm and SO_4 ranging from 710 to 1940 mg/l. concentrations of Fe, Mn, and Al also ranged widely for the West Virginia influents. In contrast, the influent to the Pennsylvania ALDs was slightly oxic (DO 1–3 mg/l) and dilute, with SC 430 μS/cm, SO_4 240 mg/l, and Fe, Mn, and Al $<$ 4 mg/l.

All the ALDs produced net alkaline effluents having pH $>$ 6 (Table 1). Generally, as the water flowed through the drains, pH, alkalinity, and concentrations of Ca increased, acidity and concentrations of dissolved Fe^{3+} (as computed by WATEQ4F), Al, and SiO_2 decreased, and concentrations of SO_4, Fe^{2+}, Mg, and Mn did not change appreciably.

Within the West Virginia drains, DO concentrations declined with depth from the air/water interface to suboxic ($<$0.5 mg/l) conditions at the bottom of the drain (Fig. 1). In the Red drain, Ca, pH, and alkalinity increased downflow, while sulfate, Al, and Fe decreased (Table 1). In the Black drain, water chemistry changed significantly between the inflow and 3.0 m downflow, whereas little change occurred from 3.0 m to the outflow at 21.3 m. From the inflow to 3.0 m, pH, alkalinity, and Ca increased, whereas SO_4, Fe, and Al declined (Table 1). In response to decline in sulfate, the water had the distinct odor of hydrogen sulfide. In the White drain, pH, alkalinity, and Ca concentrations did not change between the inflow and sampling port 15.2 m downflow. However, increased acidity and concentrations of SO_4, SiO_2, Al, Fe, and Mn (Table 1) could indicate that additional AMD enters the White drain between the inflow and the port 15.2 m downflow. At the effluent, pH, alkalinity, and Ca increased, SiO_2 decreased slightly, and Al decreased (from 34 to $<$ 1 mg/l) and was being stored in the drain.

Water throughout the Pennsylvania drains typically had DO of about 2 mg/l and was therefore at the oxic/suboxic boundary. Ca concentrations, pH, and alkalinity increased downflow, whereas Fe declined rapidly and Al declined less

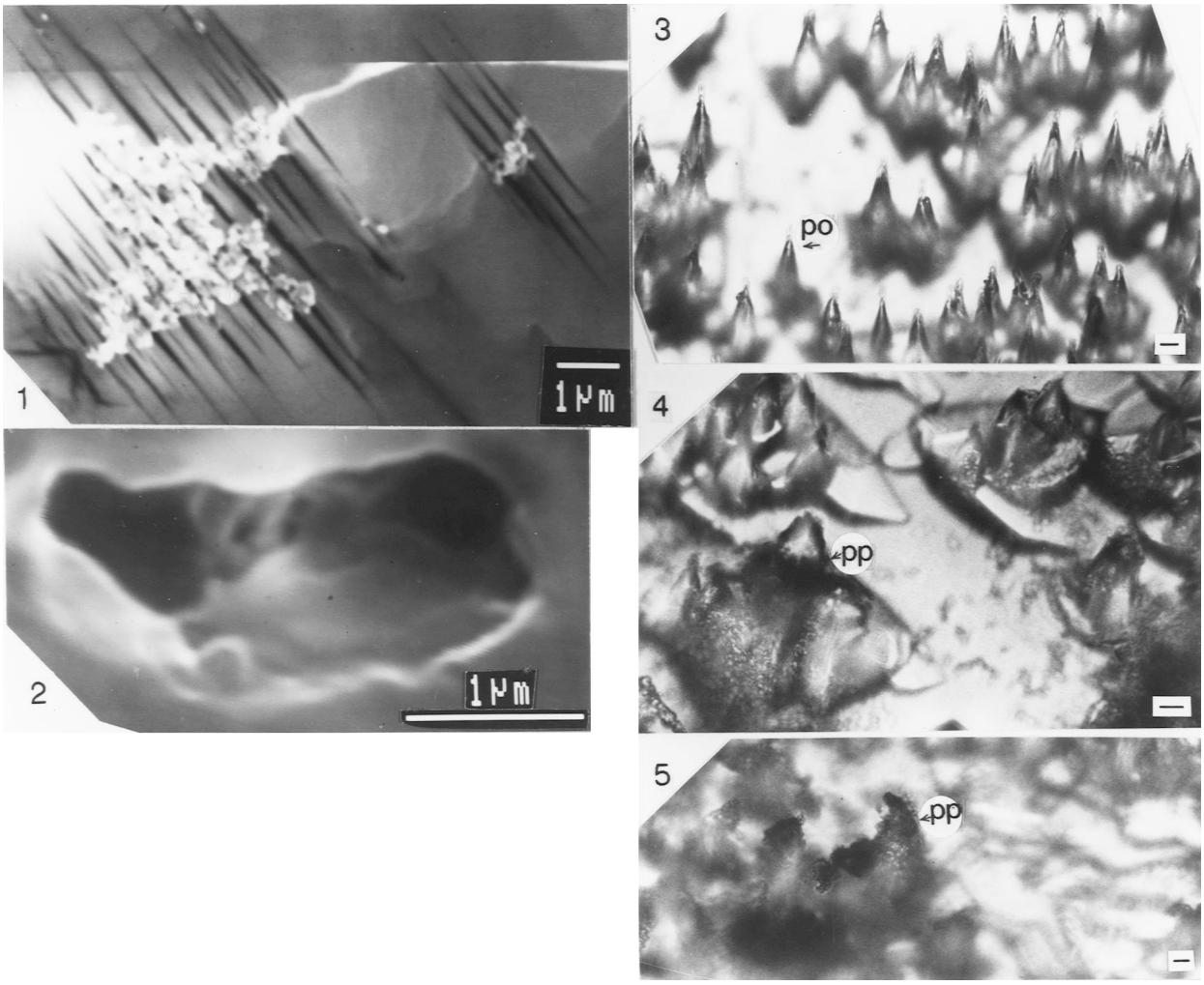

Fig. 2. Dissolution and precipitation features of gypsum and calcite (see Table 2 for explanation of sample numbers). Scale bar 10 μm unless otherwise noted. Gypsum: (1) striations visible below fluffy biofilm (Sample 23, SEM); (2) etched hole (Sample 11, SEM). Calcite: (3) etch points (po) uncoated by extraneous precipitate (Sample 1); (4) white precipitate (pp) beginning to coat etch points (Sample 3); (5) white precipitate (pp) coating calcite etch points (Sample 3)

precipitously to near detection limits along the length of the drains (Table 1).

4.3. Potential for mineral dissolution and precipitation

The computed saturation indices indicate that calcite would tend to dissolve throughout the drains, and neither Ca nor SO_4 would be likely to precipitate in most of the ALDs because the water generally is undersaturated with respect to both calcite and gypsum (Table 1). In the Red drain, gypsum saturation (SI = − 0.1) was achieved. However, as pH increased within the drains, Fe^{3+} and Al would likely undergo hydrolysis and precipitate as hydroxide or hydroxysulfate compounds. The composition and saturation indices for effluents from the West Virginia drains (Table 1) are similar to previous data [5], despite the passage of almost 4 years.

When activity of Al (pAl^{3+}) is plotted against pH (Fig. 4*A*) for the West Virginia and Pennsylvania drains, two linear trends having a break in slope around pH 4.6 match similarly plotted data by Nordstrom and Ball [12]. The [Al] versus [SO_4] plot (Fig. 4*B*) shows three clusters of data. In the concentration extreme, the data from the acidic West Virginia drains (pH 2.4–3.5) align and have a 0.31 slope ([Al]:[SO4] ≈ 1:3). The neutralized water of the West Virginia drains (pH 6.0–6.5) does not show a relation with declining SO_4. In contrast, the data for acidic to neutralized water from the Pennsylvania drains (pH 3.5–6.5) show Al declines while SO_4 remains constant.

These trends can be attributed to the formation of Al-hydroxysulfate(s) in the West Virginia drains and Al-hydroxide(s) in the Pennsylvania drains as pH increased along the flow paths. Chemical reactions due to acid neutralization by $CaCO_3$ dominate in the subsurface ALDs, in contrast to Nordstrom and Ball [12], where dilution and mixing of surface waters were the primary cause of the observed trends. Their finding that the predominant control for Al is the formation of Al-hydroxide(s) at pH > 4.6 is consistent

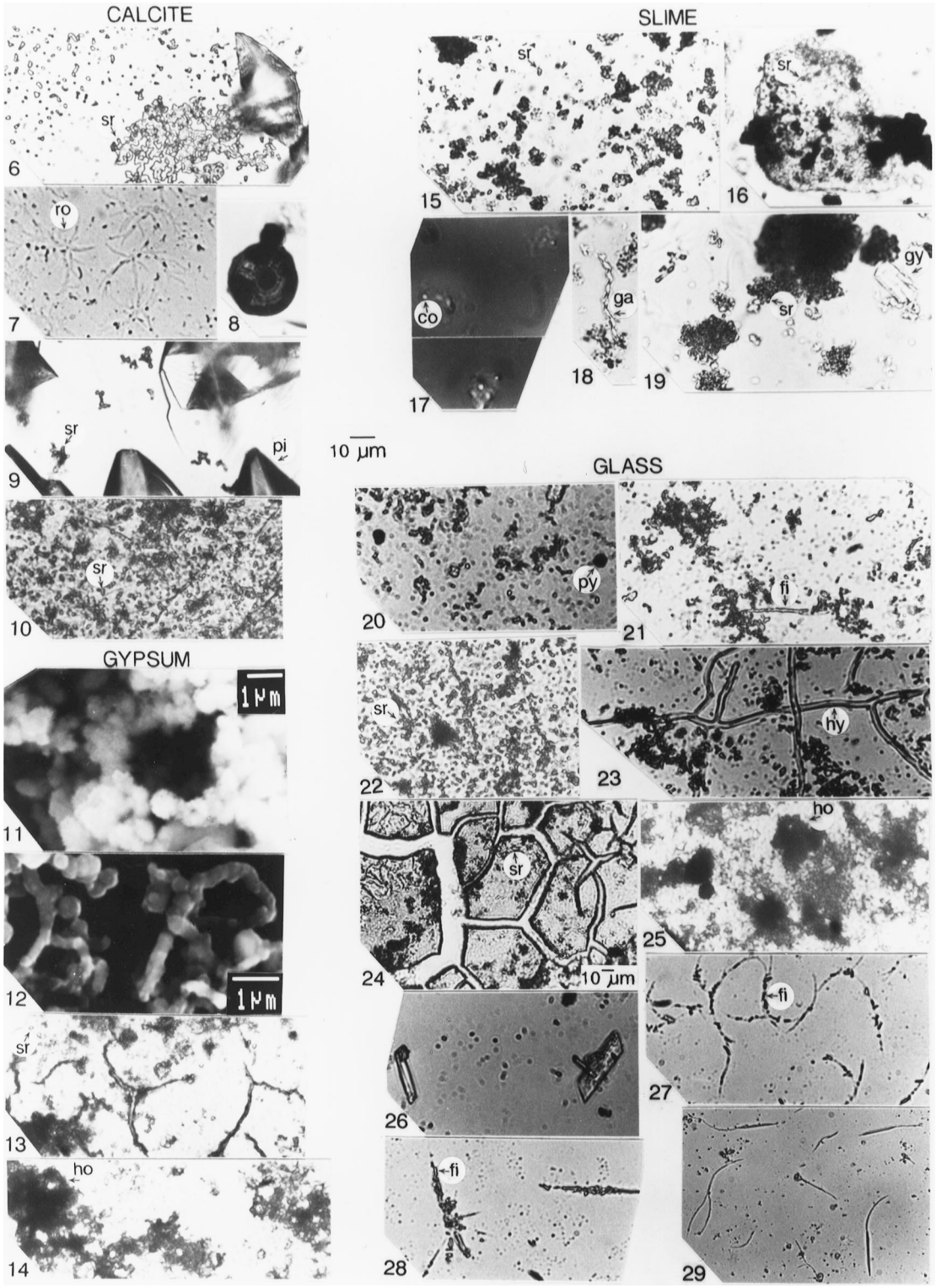
CALCITE
SLIME
GLASS
GYPSUM
sr
ro
co
ga
gy
pi
py
fi
hy
ho
6
7
8
9
10
11
12
13
14
15
16
17
18
19
20
21
22
23
24
25
26
27
28
29
10 µm
1 µm

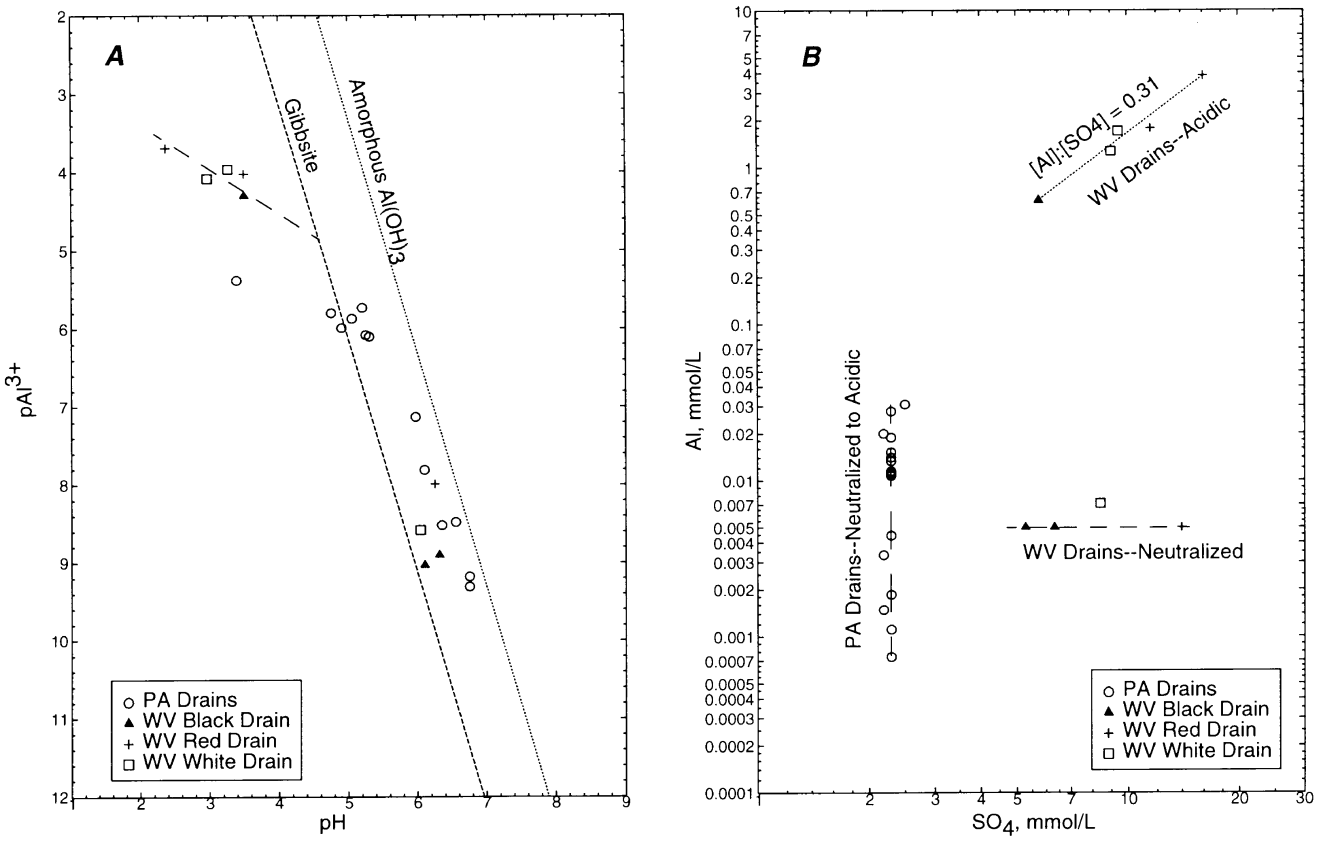

Fig. 4. Chemical data for water samples from inflow, outflow, and intermediate points within limestone drains in West Virginia (WV) and Pennsylvania (PA). (*A*) Activity of aluminum (pAl^{3+}) relative to pH. Parallel, short-dashed lines indicate solubilities for amorphous $Al(OH)_3$ and gibbsite at 1 atm and 12°C (thermodynamic data from Ball and Nordstrom [28]). Long-dashed line indicates trend for WV samples undersaturated with respect to $Al(OH)_3$ (pH < 4.6). (*B*) Relations between molar concentrations of aluminum and sulfate. Note that for the 'WV Drains neutralized' group, line at detection limit for Al (= 0.005 mmol/l) for these samples

with our data for the Pennsylvania drains and for the downflow parts of the West Virginia drains. However, under the acidic conditions (pH < 4.6) in the upflow parts of the West Virginia drains, formation of an Al-hydroxysulfate aluminite-type mineral apparently controls the concentration of Al.

4.4. Observed mineral reactions and microbial associations

Numerous, morphologically distinct bacteria were present in flocculates and attached to glass, calcite, and gypsum surfaces (Table 2, Fig. 2). Many were associated with mineral precipitates and dissolution features, which suggests active or passive microbial involvement with mineral formation and dissolution.

4.4.1. Red drain

Limestone retrieved 3.0 m from the influent was coated with brown and yellow short rods and red iron hydroxide (protoferrihydrite?) reminiscent of that analyzed by Sawicki *et al*. [33]. Calcite dissolution was evident as pits and points (Fig. 2(3)) after 20 days of immersion;

Fig. 3. Photomicrographs of microbes and precipitates (light microscope; see Table 2 for explanation of sample numbers). Scale bar 10 μm unless otherwise noted. Abbreviations: co, cocci; fi, filament; gy, gypsum; ho, holdfasts; hy, hyphae; pi, pits; py, pyrite; ro, rosettes; sr, short rods). (6) Short rods etched into calcite (Sample 3); (7) rosette-shaped features formed by rods on calcite (Sample 5); (8) fruiting body of Mn-rich fungus on calcite (Sample 17); (9) short brown rods on calcite, the large features are pits (pi) (Sample 1); (10) surface of calcite coated by numerous short brown rods (Sample 17); (11) fuzzy iron-oxide spheres on gypsum (Sample 11); (12) filaments made by cocci on gypsum (Sample 23); (13) short brown rods on biofilm having cracks on gypsum (Sample 23); (14) brown holdfasts on gypsum reminiscent of these of *Leptothrix discophora* (Sample 11); (15) brown and yellow short rods in slime (Sample 27); (16) brown and black short rods on mineral grain in slime (Sample 29); (17) cocci in slime fluorescing from acridine orange (Sample 28); (18) entwined stalk of *Gallionella* (ga) in slime (Sample 25); (19) brown short rods and degraded gypsum in slime (Sample 26); (20) pyrite framboids on glass (Sample 18); (21) short brown and colorless rods and rod filaments on glass (Sample 18); (22) brown cocci and short rods on glass (Sample 10); (23) fungal hypha colonizing glass (Sample 14); (24) acidic-type cracks in biofilm having short colorless rods on glass (Sample 16); (25) holdfasts reminiscent of *Leptothrix discophora* on glass (Sample 12); (26) gypsum precipitating on glass (Sample 16); (27) bifurcating rod filaments on glass (Sample 2); (28) filaments in process of forming gypsum on glass (Sample 8); (29) tail-like features on prismatic crystals (gypsum?) (Sample 6)

microbial colonization of the calcite was dominated by brown short rods, although cocci and other rods were also present. Microbial filaments were lined with gypsum microcrystals (Fig. 3(28)), which suggests microbial involvement with their formation. Glass surfaces were colonized by unidentified colorless bifurcating rod filaments, along with cocci and long rods.

4.4.2. Black drain

Limestone retrieved 3.0 m from the influent was coated with a slimy black iron sulfide precipitate, as well as brown and black short rods (Fig. 3(16)) which are probably sulfate-reducing bacteria. Calcite did not show dissolution after 20 days of immersion, but newly formed gypsum crystals were present; microbial colonization was dominated by brown short rods, although rosette-shaped unidentified filaments were also present. Gypsum dissolution took the form of bacteria-size holes (Fig. 2(2)); gypsum was also coated with a wide variety of microbial morphologies, including fuzzy iron-oxide spheres reminiscent of bacteria and holdfasts of the Mn-depositing *Leptothrix discophora* [32]. Glass surfaces were colonized by short rods and prismatic gypsum-like crystals which had curvilinear 'tails' (Fig. 3(29)), suggesting microbial involvement in their formation.

4.4.3. White drain

Limestone retrieved 15.2 m from the inflow was completely covered with a slimy, white aluminite-like precipitate that forms a network of interlocked spheres and rod-shaped prisms [8, 22]; silica, which is not part of the structure of the aluminite-like phase, appears to cement the crystals and occlude the pore spaces [8]. The precipitate was dominated by yellow cocci; staining by the nucleic acid dye, Acridine Orange, confirmed the slime contained cocci and rod-shaped bacteria [8]. Rod-shaped bacteria such as *Bacillus subtilis* have been noted to form such Al-bearing minerals [34]. Calcite was coated with a mosaic of white precipitate after 20 days of immersion; dissolution features included pits and points and bacteria-size holes. The points were coated with the white precipitate (Fig. 2(4)Fig. 2(5)), which suggests that dissolution preceded secondary mineral precipitation. Microbial colonization of the calcite included a colorless biofilm and brown rods; calcite was also colonized by a filamentous bifurcating *Thiothrix*-type colorless sulfur-oxidizer, suggesting the presence of a suboxic microenvironment near the crystal surface. Glass surfaces were dominated by colorless and brown rods and cocci.

4.4.4. Pennsylvania drains

Brown short rods dominated the microbial population of all substrates. Limestone and other surfaces at the inflows were coated with loosely bound, yellow-orange schwertmannite and goethite (identified by J.M. Bigham, written communication, 1997) [10, 23, 24], along with stalks of the ferrihydrite-producing iron bacterium, *Gallionella ferruginea* [35]; limestone was uncoated at 6.1 m. Calcite surfaces from the inflow to 12.2 m downflow were a mosaic of dissolution pits and points interspersed with a yellow biofilm and gypsum crystals; calcite was predominantly colonized by short brown rods and coccus filaments along with Mn-coated fungi (Fig. 3(8)). Gypsum dissolution features included striations underlying biofilms (Fig. 2(1)). Glass surfaces had pyrite or gypsum crystals along with short colorless or brown rods.

4.5. Hydrobiogeochemical interactions

4.5.1. Red drain

Increasing pH, alkalinity, and Ca downflow indicate that limestone in the Red drain is dissolving despite formation of iron-hydroxide coatings. Although the drain is suboxic, Fe^{3+} in the low-pH influent precipitated on the limestone as pH increased inside the drain. Concentrations of sulfate in the effluent were decreased by about 20% relative to influent. Hence, the gypsum crystals on calcite probably formed *in situ* considering that (a) sulfate concentrations declined while Ca concentration increased, (b) gypsum saturation was achieved (SI = −0.1), and (c) gypsum microcrystals were associated with *in situ* microbial filaments. The sulfate also could have been diluted by inflowing water and/or removed by sorption/coprecipitation with Fe–Al minerals [36–38].

4.5.2. Black drain

The water in the Black drain was undersaturated with respect to gypsum, which is consistent with microscopic dissolution features on gypsum and inconsistent with the presence of gypsum crystals on the calcite and glass surface. Random gypsum crystals not associated with bacteria probably formed as a result of evaporation after slides were removed from the drain. The formation of pyrite on gypsum indicates reducing conditions in the ALD conducive to sulfate reduction. The near-neutral pH in the drain would favor bacterial sulfate reduction [39, 40], which is consistent with the presence of brown- and black-coated bacteria that are probably sulfate reducers.

4.5.3. White drain

Limestone dissolution was limited by the encrustation and accumulation of the aluminite-like phase in the White drain because pH, alkalinity, and Ca did not increase appreciably from the inflow to the sampling port 3 m downflow where the mineral had accumulated. Furthermore, the white Al-hydroxysulfate precipitate on the calcite (Figs. 2(4) and 2(5)) isolates the chemically active surfaces from further dissolution. Bacteria typical of suboxic conditions are present and may be accelerating drain failure by oxidizing sulfide to sulfate locally or interacting with minerals that encrust limestone and restrict permeability through the drain.

4.5.4. Pennsylvania drains

Although calculations based on water chemistry indicated that gypsum and calcite were undersaturated in the two Pennsylvania ALDs, gypsum crystals along with Al-rich spheres were identified on calcite surfaces. Some of the gypsum probably formed as a result of evaporation as the slides were removed from the drain, particularly where gypsum crystals were random and not associated with microbial filaments. Bacteria and fungi colonizing calcite and gypsum surfaces may be contributing to the formation of microenvironments conducive to mineral dissolution and precipitation. Etch pits on calcite surfaces and higher alkalinity within zones of Fe–Al–SiO_2 accumulation indicate calcite dissolution was not inhibited despite the formation of secondary minerals and biofilms. Nevertheless, the accumulation of Fe and Al precipitates suggests that flow rates and paths through the Pennsylvania ALDs could eventually be affected.

5. Conclusions

(1) In general, white Al-bearing precipitates formed in all the ALDs; however, failure due to clogging was observed only for the drains receiving high metal loads. Clogging would be most likely for situations where the load is high due to high concentrations and low flow rates, because rapid flow rates may flush some precipitates from the ALDs.

(2) For this study and ALDs in general [5], Al concentrations were lowest near the known Al solubility minimum at pH 5–6 [12, 41]. This suggests that a pre-treatment step to adjust pH in the range of 5–6 without oxygenating the water might be appropriate for the removal of Al before acidic mine drainage is introduced in the subsurface to alkalinity producing materials such as limestone, CCBs, and FGDBs. The high Al content of these materials would not be a concern as long as the target pH was maintained.

(3) The formation of secondary Al, Fe, and Mn minerals on calcite was consistently associated with growth of microorganisms. Bacteria and fungi coating mineral surfaces can significantly affect precipitation and dissolution. Additional studies are required to discern the specific role(s) of bacteria in the formation of Al-hydroxysulfate precipitates and for development of field methods to minimize fouling associated with microbial and mineral growths in ALDs. The very large variability of microbial populations on the homogenous substances tested in this research suggest that reactions with heterogenous alkalinity-producing materials such as CCBs and FGDBs will be difficult to predict in advance of performing the actual field tests.

Acknowledgements

We thank K.A. Balciauskas, B. Barker, H.E. Belkin, J.M. Bigham, K.M. Briggs, J.J. Donovan, F.T. Dulong, J.I. Eddy, C.D. Gullett, K.J.T. Livi, T.A. Ridley, and M.K. Trahan for field and laboratory assistance, and D.K. Nordstrom for sharing ideas on data interpretation.

References

[1] Aljoe WW. In: Proceedings, 13th Annual Meeting of American Society for Surface Mining and Reclamation, Knoxville, TN, 1996:827.
[2] Schueck J, DiMatteo M, Scheetz B, Silsbee M. In: Proceedings, 13th Annual Meeting of American Society for Surface Mining and Reclamation, Knoxville, TN, 1996:308.
[3] Haefner RJ, Rowe GL. US Geological Survey Fact Sheet FS-051-97, 1997.
[4] Hedin RS, Nairn RW, Kleinmann RLP. US Bureau of Mines Information Circular IC-9389, 1994.
[5] Hedin RS, Watzlaf GR. In: US Bureau of Mines Special Publication SP 06A-94, International Land Reclamation and Mine Drainage Conference and 3rd International Conference on the Abatement of Acidic Drainage, vol. 1, 1994:185.
[6] Skousen JG, Faulkner BB. In: Proceedings, 13th Annual Meeting of West Virginia Surface Mine Drainage Task Force, West Virginia University, Morgantown, WV, 1992.
[7] Skousen JG, Ziemkiewicz PF. Acid mine drainage control and treatment. Morgantown, WV: West Virginia Univ., 1995.
[8] Robbins EI, Nord GL, Savela CE, Eddy JI, Livi KJT, Gullett CD, Nordstrom DK, Chou I-M, Briggs KM. In: Chiang S-H, editor, Coal-energy and the environment. Proceedings, 13th Annual International Pittsburgh Coal Conference, vol. 2, 1996:761.
[9] Bertsch PM, Miller WP, Anderson MA, Zelazny LW. Clays and Clay Minerals 1989;37:12.
[10] Bigham JM, Schwertmann U, Traina SJ, Winland RL, Wolf M. Geochimica et Cosmochimica Acta 1996;60:2111.
[11] Nordstrom DK, Alpers CN. The environmental geochemistry of mineral deposits—Part, A., processes, methods, and health issues. In: Plumlee GS, Logsdon MJ, editors. Reviews in Economic Geology, vol. 6, in press.
[12] Nordstrom DK, Ball JW. Science 1986;232:54.
[13] Ott AN. US Geological Survey Water-Resources Investigations Report 84-4335, 1986.
[14] Karathanasis AD, Evangelou VP, Thompson YL. Journal of Environmental Quality 1988;17:534.
[15] Karathanasis AD, Thompson YL, Evangelou VP. Journal of Environmental Quality 1990;19:389.
[16] Ferris FG, Tazaki K, Fyfe WS. Chemical Geology 1989;74:321.
[17] MacInnis IN, Brantley SI. Geochimica et Cosmochimica Acta 1992;56:1113.
[18] Morse JW. Carbonates-mineralogy and chemistry. In: Reeder RJ, editor. Reviews in mineralogy, vol. 11. Mineralogical Society of America, 1983:227.
[19] Plummer LN, Parkhurst DL, Wigley ML. Chemical modeling in aqueous systems-speciation, sorption, solubility, and kinetics. In: Jenne EA, editor. American Society Symposium Series 93, 1979:537.
[20] Ghiorse WC, Wilson JT. Advances in Applied Microbiology 1988;33:107.
[21] Robbins EI, Cravotta CA III, Savela CE, Nord GL Jr, Balciauskas, Belkin HE. In: International Ash Utilization Symposium, Lexington, KY, 1997:546.
[22] Nord GL Jr., Robbins EI, Livi KJT. US Geological Survey Open-File Report OF97-496. In: 4th International Symposium on Environmental Geochemistry, 1997:67.
[23] Cravotta CA III, Trahan MK. In Proceedings, 13th Annual Meeting of American Society for Surface Mining and Reclamation, Knoxville, TN, 1996:836.
[24] Cravotta CA III, Trahan MK. Applied Geochemistry (in press).
[25] Nordstrom DK. Geochimica et Cosmochimica Acta 1977;41:1835.

[26] Wood WW. US Geological Survey Techniques of Water Resources Investigations, Book 1, Chapter D2, 1976.
[27] Fishman MJ, Friedman LC, editors. US Geological Survey Techniques of Water-Resources Investigations, Book 5, Chapter A1, 1989.
[28] Ball JW, Nordstrom DK. US Geological Survey Open-File Report 91-183, 1991.
[29] Zobell CE. Journal of Bacteriology 1943;46:39.
[30] Mills AL, Mallory LM. Microbial Ecology 1987;14:219.
[31] Greenberg AE, Clesceri LS, Eaton AD, Franson MAH, editors. In: Standard Methods for the Examination of Water and Wastewater (18th), Section 9240. Washington, DC: American Public Health Association, 1992.
[32] Robbins EI, Norden AW. Coal-energy and the environment. In: Chiang S-H, editor. Proceedings, 11th Annual International Pittsburgh Coal Conference, vol. 2, 1994:1154.
[33] Sawicki JA, Brown DA, Beveridge TJ. Canadian Mineralogist 1995;33:1.
[34] Urrutia MM, Beveridge TJ. Geoderma 1995;65:149.
[35] Chukhrov FV, Zvyagin BB, Gorshkov AI, Yermilova LP, Balashova VV. International Geology Reviews 1974;16:1131.
[36] Ali MA, Dzombak DA. Geochimica et Cosmochimica 1996;60:5045.
[37] Nordstrom DK. Geochimica et Cosmochimica Acta 1982;46:681.
[38] Rose S, Ghazi AM. Environmental Science and Technology 1997;31.
[39] Chapelle FH. Ground-water microbiology and geochemistry. New York: Wiley, 1993.
[40] Ehrlich HL. Geomicrobiology, 2nd ed. New York: Marcel Dekker, 1990.
[41] Hem JD. US Geological Survey Water-Supply Paper 2254, 1985.